



## DISCUSSION OF FRACTURE CRITERIA IN SPALL MECHANICS

P. CHEVRIER and J.R. KLEPACZKO (METZ)

An analysis of variety of spall criteria is discussed in this paper. Some mechanisms of the free surface creation in spall are discussed, including cleavage and fibrous separation. Existence of those micromechanisms of fracturing is illustrated by several fractograms for aluminum alloy, iron and steel. Finally, three groups of fracture criteria used in prediction of spalling are reviewed. It is concluded that all modern spall criteria must have an evolutionary character, that is they must take into account the time evolution of damage. A relatively new simple criterion based on the Boltzmann statistics is verified for 7020-T6 aluminum alloy. This simple criterion appeared to be quite efficient in finite elements computer codes.

### 1. INTRODUCTION; FRACTURE CRITERIA

It is well known that all processes of fracturing, elastic or elasto-plastic are rate and temperature-dependent. The most general means for estimating the microstructural weakening, and in consequence the microcrack or microvoid formation, is a consideration of the energetics of less resistant microvolumes in a material. The local stress components  $\sigma_{ij}$  produce a strain energy density in a material. Thus, a fracture criterion must take into account not only the local strain rate and temperature but also the local stress distribution. The local fracture criteria are based on this concept. For example, the critical conditions are reached, and a crack will propagate, when some specified parameters exceed some characteristic values in the process zone, that is in the microvolume where the free surfaces are created. A simple classification of the local approaches in fracture mechanics can be found, for example, in [1]. If an isolated crack is already present, two local fracture criteria are most frequently used:

i)  $\sigma_{22} = \sigma_F$  at  $x_1 = l_F$ , i.e., the stress  $\sigma_{22}$  normal to the crack plane must be equal to the local fracture stress  $\sigma_F$  at the characteristic in-plane distance  $l_F$  from the crack tip.

ii)  $\varepsilon_{22} = \varepsilon_F$  at  $x_1 = l_F$ , i.e., the normal strain  $\varepsilon_{22}$  must be equal to the critical strain  $\varepsilon_F$  at the characteristic in-plane distance from the crack tip.

Another criterion, derived from i), is the following:

iii)  $\sigma_n^{\max} = \sigma_F$ , the maximum normal stress  $\sigma_n^{\max}$  at constant hydrostatic pressure  $p$  must be equal to the critical fracture stress  $\sigma_F$ .

This last criterion is quite useful in all fracture processes of spalling where the characteristic distance is unspecified and the hydrostatic component of the stress tensor is well defined. The main advantage of the local criteria is that they specify to some extent the local, or “microscopic”, conditions in the process zone when the new free surfaces are created. Thus, some physical parameters like grain size can be taken into account in the local approach. It may be mentioned that the local criteria are very useful in computational fracture mechanics.

Different physical mechanisms involved in the processes of fracturing cause that the fracture mechanics lacks certain universal criteria. Investigation of physical reasons of fracture mechanisms base largely on fractography, that is optical microscopy and electron microscopy, mostly scanning. With an introduction of observation techniques based on scanning electron microscopy it has become possible to monitor fracture surfaces directly. Further progress in scanning electron microscopy is related to the image analysis with direct application of statistical methods.

Fractography has revealed a variety of micromechanisms of material separation. The most common is classification as brittle or ductile fracture. Those definitions are not so precise, and further classification of fracture morphologies are possible, for example:

- i) surface separation by cleavage (“brittle” process):
  - a. quasi-cleavage,
  - b. intergranular cracking,
  - c. transgranular cracking.
- ii) fibrous separation (“ductile” process):
  - b. microvoid coalescence,
  - c. adiabatic shear bridges.

It is commonly assumed that mechanisms of separation associated with cleavage are controlled by the critical cleavage stress  $\sigma_F$ , whereas all fibrous mechanisms of separation are controlled by the local critical strain  $\varepsilon_F$ . An ideal cleavage fracture of metallic grains or single crystals occurs by direct separation along crystallographic planes oriented most favorably according to the maximum normal stress  $\sigma_n^{\max}$ . The mechanism of cleavage is typical of low temperatures and short time loading, ranging from milliseconds to nanoseconds. In general, the cleavage fracture dominates in BCC crystallographic structures. Very frequently the cleavage is combined with twinning. As a whole, the mechanism of cleavage is not very sensitive to changes of temperature and loading rates.

The simplest approach to estimate main factors associated with the cleavage fracture is due to GRIFFITH [2]. It has been postulated that a crack already exists and during increment of crack length  $da$ , the sum of the potential elastic energy of deformation and the surface energy is constant. If  $\gamma$  denotes the surface energy density, then the critical stress at fracture of a brittle material is:

$$(1) \quad \sigma_F = \sqrt{\frac{2\gamma E}{\pi a_c}},$$

where  $E$  is the Young modulus, and  $a_c$  is the critical crack length. This criterion, known as the Griffith criterion, can be recognized as the local one. However, the existence of microcracks, or flaws, in a body, has been assumed in advance.

In metallic materials a structural weakening occurs due to existence of interfaces, for example grain boundaries. The fragility of interfaces may decrease the critical stress  $\sigma_F$  predicted by Eq. (1). A simple generalization of the Griffith criterion where the fragility of interfaces was taken into consideration is due to GILMAN [3]. The applied normal stress  $\sigma_n$  produces a strain energy density in the material  $W_\varepsilon = \sigma^2/2E$ . Introduction of a microcrack of length  $2L$  causes that the strain energy  $W_\varepsilon$  in a volume  $\sim \pi L^2$  (for the unit thickness) is released. This amount of energy is:

$$(2) \quad W_\varepsilon = - \left( \frac{\pi \sigma^2 L^2}{2E} \right).$$

Further, some of the interfaces are eliminated by this process and its energy is  $W_i = -2L\gamma_i$ , where  $\gamma_i$  is the specific interfacial energy. Finally, two new surfaces of area per unit thickness  $4L$  are created. The energy required to produce a free surface when there is no interface is called specific surface energy  $\gamma_s$ . The energy increase associated with the new surface is  $W_s = 4L\gamma_s$ .

The critical stress that is required for a crack growth along an interface is found by a similar procedure as that used by Griffith, and is given by:

$$(3) \quad \sigma_{Fi} = \sqrt{\frac{4E}{\pi L_c} \left( \gamma_s - \frac{1}{2}\gamma_i \right)}.$$

If there is no interface,  $\gamma_i = 0$ , the fracture stress is the same as predicted by Eq. (1), with  $L_c = 2a_c$ . The ratio of the critical stresses can be estimated as:

$$(4) \quad \frac{\sigma_{Fi}}{\sigma_F} = \sqrt{1 - \frac{\gamma_i}{2\gamma_s}}.$$

This ratio eliminates automatically the details of interface geometry and the elastic stiffness of the matrix. It is interesting to note that no matter what the

geometry of interface, the strength tends to zero as the magnitude of the interface energy  $\gamma_i$  approaches twice that of the surface energy  $\gamma_s$ . It is known that for pure metals, the effect of grain boundaries on  $\sigma_F$  is not large. The typical value of the ratio, Eq. (4), is around 0.9.

In case of alloys or impure metals, layers of foreign atoms may exist at grain boundaries. This generally increases  $\sigma_F$ , but suppression of the local plastic flow can substantially reduce the fracture surface energy and produce more brittleness. On the other hand, any dilatation present near the grain boundaries produces the weakening effect and the critical stress  $\sigma_F$  decreases very rapidly, [3]. This effect on  $\sigma_F$  can be estimated by changes of the atomic density  $\rho_a$ , defined by the number of atoms per unit volume,

$$(5) \quad \frac{\Delta\sigma_F}{\sigma_F} = \frac{4}{3} \left( \frac{\Delta\rho_a}{\rho_a} \right),$$

where  $\Delta\rho_a$  is caused by the local changes in the atomic spacing along the grain boundaries due to dilatation. This effect may be quite important for high-strength materials, [3]. Such constraint effect on the brittle fracture may have some consequences in spall mechanics where the local dilatation may reach a high level.

It is also known that polycrystalline metals often fracture intergranularly, but in this case the impurities are usually segregated at the grain boundaries. Metals and alloys never fracture in a pure brittle mode, some local plastic deformation always precedes fracture and this complicates the role of grain boundaries in the brittle fracture. In the case of spalling the local stress rates are very high, so the time available to develop local plastic deformation prior to fracture is very limited. This is why the spall surfaces tend to show more cleavage facets. In general, fracture processes at high loading rates are more brittle.

## 2. REMARKS ON DUCTILE FRACTURE

In spalling, the microcrack dynamics is the key factor for understanding the cleavage separation at different loading rates and temperatures. The Griffith-Orowan formulation is more representative, and more exact in the case of metals when a correction for the surface energy is introduced which takes into account a small amount of plastic work almost always present during quasi-cleavage separation. Equation (1) can be rewritten in the following form

$$(6) \quad \sigma_F = \sqrt{\frac{\xi E(\gamma_e + \gamma_p(\dot{\epsilon}, T))}{(1 - \nu^2)a_c}}$$

with  $\xi = \pi/2$  and  $\xi = 2/\pi$  respectively for the penny-shaped, and through-thickness microcracks, the total surface energy  $\gamma$  is split into elastic  $\gamma_e$  and plastic part  $\gamma_p$ ,  $a_c$  is the half-length of a crack. The fictitious surface energy  $\gamma_p$  due to plastic work expended during quasi-cleavage separation is very low at low temperatures and the critical cleavage stress  $\sigma_F$  remains nearly constant, independent of the loading rate or temperature. Typical values for steels are:  $0.8 \text{ GPa} \leq \sigma_F \leq 3.8 \text{ GPa}$ . At higher temperatures the plastic work may contribute more extensively to the separation process and, consequently,  $\sigma_F$  becomes more rate and temperature-dependent. Indeed, at room temperature the critical stress  $\sigma_F$  for quasi-cleavage fracture is time-dependent, [1, 4, 5].

Fracture associated with the plastic deformation within the process zone of an isolated crack is essentially ductile. Plastic deformation relaxes the constraint in the process zone and further plastic deformation is easier. The process of material separation occurs by the micromechanism of microvoid growth and coalescence. The fracture surface after such separation shows characteristic dimples. Since engineering materials always contain second phase particles, which are more brittle than the matrix, the more brittle spots initiate microvoids. Consequently, the size of dimples is related to the distribution of second phase particles. A general conclusion can be drawn that triggering of the ductile fracture is caused by the local heterogeneities. This leads to the fibrous fracture caused by growth and coalescence of voids. Since the sites of fracture initiation are spatially distributed, the local growth of voids is followed by adiabatic shearing of the ligaments. An example of the ligament shearing is shown in Fig. 1 for Al-alloy 7020-T6. In conclusion,

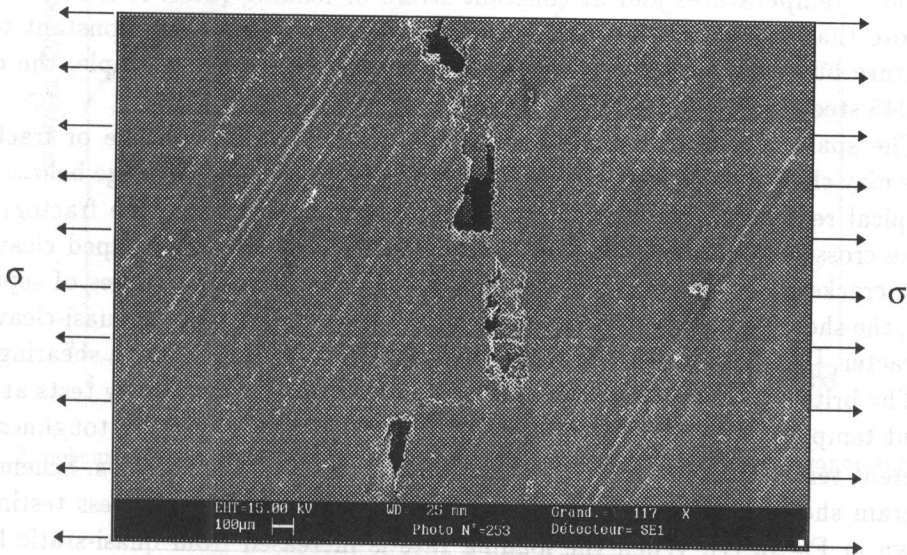


FIG. 1. Fractogram of the shear bridge after spalling of Al-alloy 7020-T6.

in the ductile fracture the plasticity is involved not in a simple and direct way. Of course, the external parameters like the loading time, temperature, hydrostatic pressure and others strongly influence the final result.

The so-called damage theories of ductile fracture are quite commonly used in quasi-static and dynamic fracture mechanics [6]. It is not intended to review such theories here, more recent advances in this field can be found, for example, in [7, 8, 9]. Application of the statistical theories of damage to spalling has been introduced in [9]. Some discussion of this approach is included later on in this paper.

### 3. BRITTLE-DUCTILE TRANSITION

Since all metallic materials exhibit rate and temperature-sensitivity of plastic properties, it is expected that fracture, or spall properties, will also depend on loading rate and temperature. One feature observed in construction materials is the brittle-to-ductile transition. The transition from brittle to ductile behaviour is observed in some construction alloys, primarily steels, independently of whether bulk specimens are tested or the notch-toughness is investigated. It should be noted that some metals and alloys, for example aluminum, aluminum alloys, titanium and titanium alloys (generally other structures than BCC) do not exhibit a transition-temperature behaviour. The transition can be studied simply by performing a series of tests (tensile or fracture tests) at different, usually low, temperatures and at constant strain or loading rates. It is interesting to note that the ductile-to-brittle transition can be observed at constant temperature but with consecutively increased loading rates. For example, the case of 1045 steel has been discussed in [1].

The spall tests may provide similar results. Quasi-static tensile or fracture tests may show ductile fracture, but the spall tests may yield cleavage behaviour, a typical representative in such conditions being Armco iron. The fractograph of the cross-section of spalled Armco iron specimen with penny-shaped cleavage microcracks is shown in Fig. 2, [4]. In addition, for advanced stages of separation, the shear ligaments between particular microcracks have also quasi-cleavage character, [10]. The process of coalescence occurs by quasi-cleavage shearing.

The brittle-to-ductile transition is easily observable after Charpy tests at different temperatures. A more modern approach is to study fracture toughness at different temperatures and loading rates, up to  $\dot{K}_I \approx 10^6 \text{ MPa}\sqrt{\text{m/s}}$ . Schematic diagram showing the brittle-ductile transition via fracture toughness testing is shown in Fig. 3, [1]. When the loading rate is increased from quasi-static level (e.g.  $\dot{K}_I \approx 1 \text{ MPa}\sqrt{\text{m/s}}$ ) to dynamic loading (typically  $\dot{K}_I \approx 10^6 \text{ MPa}\sqrt{\text{m/s}}$ ),

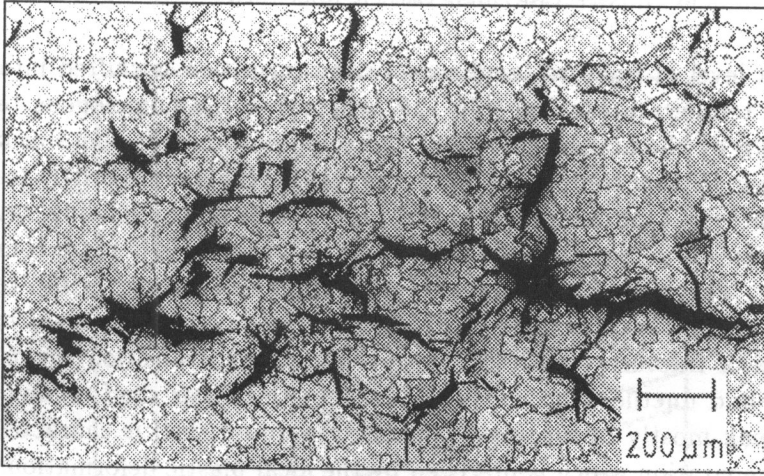


FIG. 2. Fractogram of the cross-section of Armco iron specimen with quasi-brittle microcracks, [4].

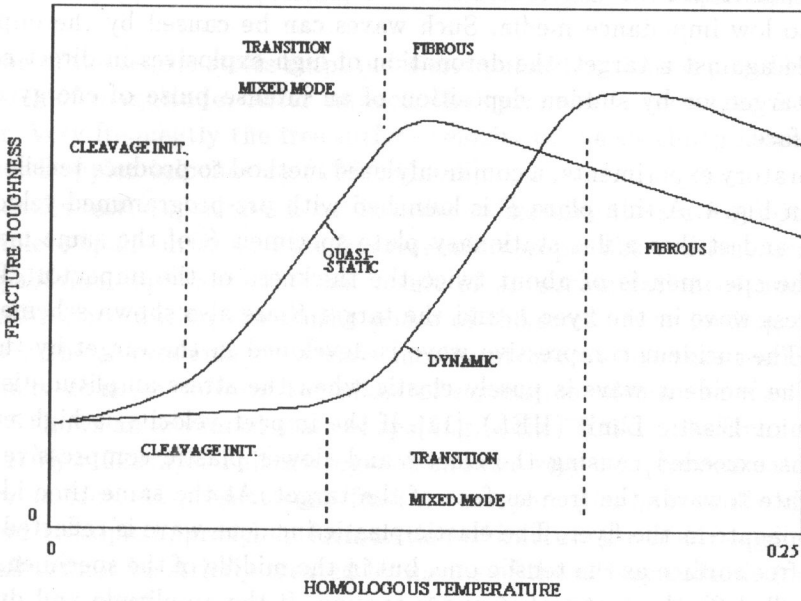


FIG. 3. Schematic changes of fracture toughness as a function of homologous temperature for two very different loading rates, [1].

the constant level of fracture toughness, or the transition is shifted into higher homologous temperatures. The shift  $\Delta\theta$ , where  $\theta$  is the homologous temperature, is shown by the horizontal arrow. The temperature shift obeys usually the Arrhenius law. Within some region of temperatures the ductile-brittle transition is possible at constant temperature only by change of the loading rate, such situation is shown in Fig. 3 by the vertical arrow. This case is more common in spall testing. The highest negative rate sensitivity is observed in the region of the transition temperature. The characteristic *S* shape of the curves indicates three modes of fracture: brittle (cleavage separation), transition range (mixed separation) and ductile (fibrous separation). In the lower shelf regime, metals or alloys break mostly by cleavage, whereas the upper shelf is characterized by the ductile separation which is preceded by the local plastic deformations. So far there is no available data on systematic analysis of ductile-brittle transition in spalling.

#### 4. PROCESS OF SPALLATION

Spallation is a specific kind of fracture in solids which is developed by tensile stress pulses produced by reflection of compression waves at the interfaces adjacent to low impedance media. Such waves can be caused by the impact of a projectile against a target, the detonation of high explosives in direct contact with the target, or by sudden deposition of an intense pulse of energy on the target surface.

In laboratory experiments, a commonly used method to produce tensile pulses is shown in Fig. 4. A thin plate *F* is launched with pre-programmed velocity by a gas gun and strikes a flat stationary plate specimen *S* of the same material. Usually the specimen is of about twice the thickness of the impactor. The reflected stress wave in the flyer *F* and the target *S* are also shown schematically in Fig. 4. The incident compressive wave is developed in the target by the flyer impact. The incident wave is purely elastic when the stress amplitude is below the Hugoniot Elastic Limit (HEL), [11]. If the impact velocity is high enough, the HEL is exceeded causing the elastic and slower plastic compressive waves to propagate towards the free surface of the target. At the same time identical waves propagate in the flyer. The elastic-plastic incident wave is reflected at the specimen free surface as the tensile one, but in the middle of the specimen, in the region labelled *T*, the material is under tension. If the amplitude and duration of the tensile reflected wave is high enough, the spall occurs in the middle of the target.

The parameters which can be varied are the impact velocity  $V_0$ , and relative specimen and impactor thickness,  $L_s$  and  $L_f$  respectively. Using this technique,

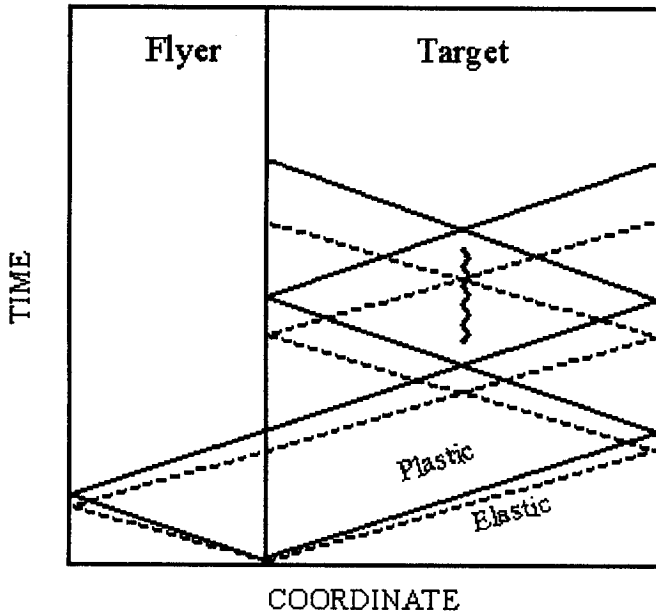


FIG. 4. Lagrangian figure showing wave patterns for plate/plate impact configuration, *F* - flyer plate, *S* - specimen, *C* - compressive region, *T* - tensile region.

variation of the tensile stress amplitudes and pulse durations is possible by about one order of magnitude. After impact, the specimen is recovered in a special catcher. Very frequently the free surface velocity of the specimen is measured by the laser-Doppler velocimetry (VISAR), [37].

After the test, a specimen is cut in order to examine the state of microdamage or complete spall surfaces. Post-fracture microscopic observations demonstrate that spallation represents the end result of an accumulation of microdamage that takes place during the tensile phase of the stress wave loading. In ductile materials the microdamage consists mostly of microvoids that nucleate, grow and finally coalesce to form the plane of separation within the material body. Figure 5 shows an advanced state of spalling in the 7020-T6 aluminum specimen tested at  $V_0 = 220$  m/s. This micrograph shows a very complicated pattern of the fracture surface. At present such fracture morphologies practically eliminate a direct microscopic approach in formulation of fracture criteria in spalling. Hence the spall cannot be strictly treated by means of the theory suitable for a simple crack. In general there are two trends to formulate the criteria of spallation. One is based on the cumulative damage modeling and the other is based on statistics of the nucleation and coalescence of microvoids or microcracks. The former deals with the problem macroscopically, the latter is a kind of statistical approach. Fracture-like scabbing is not instantaneous and a finite time is required for crack

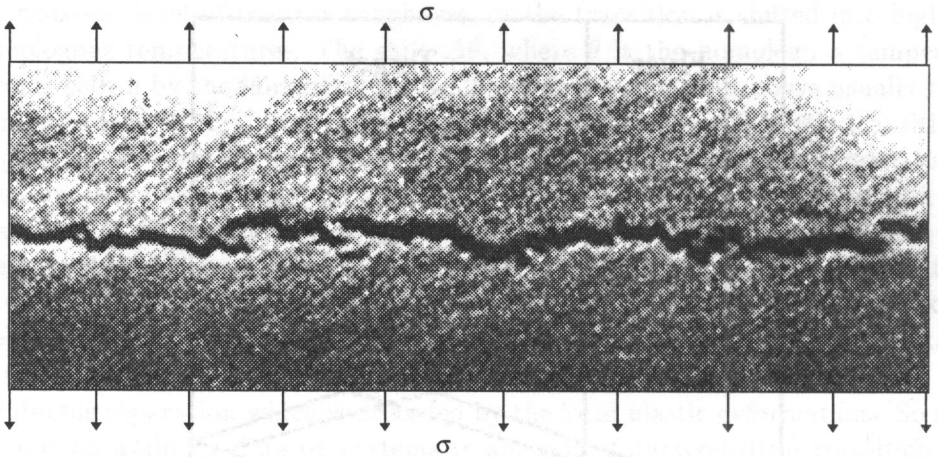


FIG. 5. Advanced state of spall in 7020-T6 aluminum alloy, impact velocity  $V_0 = 220$  m/s.

initiation. The spall process occurs within a rather short period (1 to  $0.1 \mu\text{s}$ ) and the maximum tensile stress (the spall strength) is about 2.5 times higher than the uniaxial fracture stress. The very short time and the high value of the fracture stress are the main characteristics of the spall phenomenon. The dependence of spall strength on the loading rate can be represented by the curve displayed in Fig. 6. The shape of the curve can be interpreted as an evidence of a cumulative process of the spall fracture. The spall stress  $\sigma_F$  increases when the loading rate increases, at the same time the critical time to fracture  $t_c$  diminishes. This fact is supported by the observation of fracture surfaces. Metals and alloys which separate through ductile fracture exhibit a plastic process zone in the form of layers. Within this zone, plastic growth of voids and ligament rupture occur leading to full fracture separation. Analysis of the plastic process zone leads to some degree of understanding of the transition from cleavage dominated to plasticity dominated spall. It is not clear whether the ductile-brittle transition can be precisely detected and shown in the coordinates  $\sigma_F(t_c)$ , Fig. 6. Difficulties lie also in a wide range of loading rates needed to cover the widest spectrum of the critical time  $t_c$ . In principle, at least two experimental techniques must be used, that is the plate impact and the laser energy deposition, [12, 13], see Fig. 6.

Variety of micromechanic or mesomechanic processes may be involved in the evolution of damage accumulation and spall. Some of them are discussed in the previous part of this paper. This variety causes that there is no ONE universal criterion for spalling of materials. The existing local fracture criteria, normally used in fracture dynamics, can also be used for spall estimation. However, in spall mechanics the characteristic distance, introduced in the fracture mechanics criteria, does not exist or at least is difficult to define. For the case of spall, the

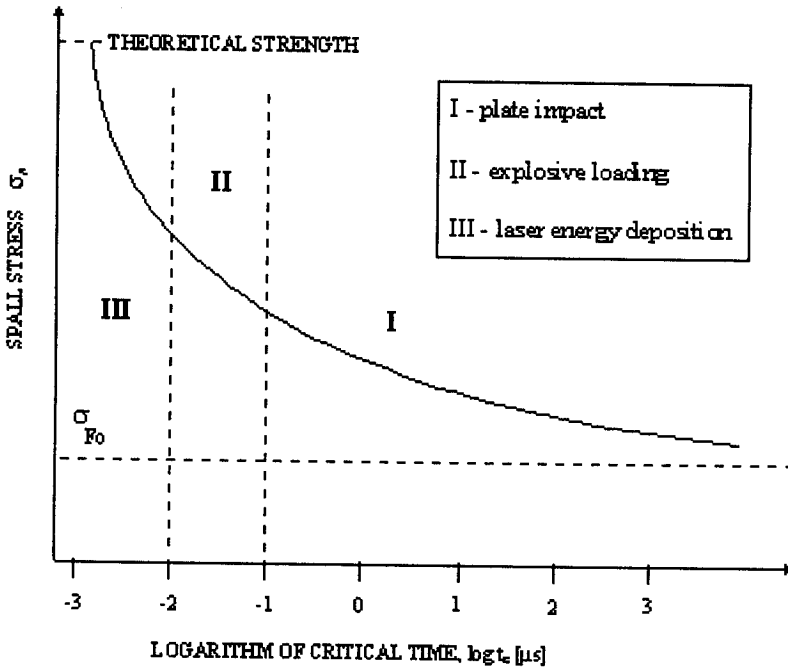


FIG. 6. Schematic display of the spall stress  $\sigma_F$  as a function of the critical time to fracture  $t_c$  ( $\mu\text{s}$ ), for a specific shape of the loading history  $\sigma_{22}(t)$ .

analysis of each microcrack individually becomes irrational. In such a case the criteria are reduced to a cumulative approach with one or more material parameters, for example  $\sigma_F(tc)$  as shown in Fig. 6, [1, 14]. A more complex mathematical approach is based on the introduction of an average microscopic evolution of microvoid density as an internal state variable, [8, 10, 12, 34]. The first approach is much easier to use in large computer codes, the second is still in the state of development and the microstatistics must be known in advance for each material under consideration. In order to summarize the state of the art in application of different criteria used in fracture dynamics (mostly local) and in spall mechanics, a literature search was undertaken and the final result is shown in Table 1. The first column contains the reference, the second authors and publication year, the third mathematical formulation, the fourth the constants and finally the fifth column contains short comments. Standard symbols like wave speed  $C_1$ , damage level  $D$ , strain  $\varepsilon$ , strain rate  $\dot{\varepsilon}$ , universal gas constant  $k$  (Boltzmann constant), density  $\rho$ , void radius  $R$ , stress  $\sigma$ , time  $t$ , absolute temperature  $T$ , mass velocity  $v$ , are not directly explained in the Table 1. Other symbols are defined in the fourth column.

## 5. AN APPLICATION TO ALUMINUM ALLOY 7020-T6

The following three stages of ductile spall are commonly observed: the incipient, intermediate and complete. Each stage can be classified according to the severity of surface separation. The incipient spall can be found only by metallographic examination at high magnification. The intermediate spall can be visible without magnification and microcracks or microvoids are larger and sometimes connected. The complete spall is defined as a free surface (complete separation). The combination of the normal stress tensile history  $\sigma_n(t)$  and the pulse duration  $t_c$  at which the complete spall occurs, defines the threshold spall values needed to define a spall criterion. Such criterion must be based on wave dynamics and delay time in material separation. Experiments do show that the process of spallation, from the incipient stage to the final separation, must be time-dependent. Simply, ductile materials require more time to create a free surface than brittle materials. Those differences are amplified by the stress relief due to the local plasticity in the process zone. It is also clear that spallation is a process with its specific kinetics. Thus, the physically plausible criteria of spalling found in the literature are based on two independent approaches. The first one proposed in Ref. [10, 17, 9] is based on time evolution of microvoid population and size, and the explicit formulation is as follows:

$$(7) \quad \frac{dN}{dt} = g(\sigma^*) \quad \text{and} \quad \frac{dR}{dt} = h(\sigma^*, R_0),$$

where  $\dot{N}(t)$  and  $\dot{R}(t)$  are respectively time-dependent evolution of the number of microvoids or cracks and its size. Both rates are increasing function of the overstress  $\sigma^* = \sigma - \sigma_0$ , where  $\sigma_0$  is the threshold stress below which no damage occurs,  $R_0$  is the initial dimension of microvoid and  $\sigma$  is the instantaneous value of the normal tensile stress. Explicit form for the cumulative damage criterion suggested in Ref. [10, 17, 9] are

$$(8) \quad \frac{dN}{dt} = \dot{N}_0 \exp\left(\frac{\sigma - \sigma_{N0}}{\sigma_1}\right) \quad \text{and} \quad \frac{dR}{dt} = \frac{(\sigma - \sigma_{R0})}{4\eta} R_0,$$

where  $\dot{N}_0$ ,  $\sigma_{N0}$ ,  $\sigma_1$ ,  $\sigma_{R0}$  and  $\eta$  are empirical constants. The formulation in [10, 17, 9] is logical but the problem of specifying the complete material parameters, including the range of microscopic voids, is clearly a formidable task. In addition this treatment is empirical and cannot be extrapolated with confidence to other materials and loading conditions. Recent progress made in quantitative fractography, for example [18], may push forward our understanding of dynamic fracture phenomenology, and particularly in development of nucleation, growth and coalescence micromechanisms. At present, applications of statistic models in

numerical schemes are difficult and sometimes even impossible, mostly because of the lack of data.

A simpler approach is based on a single evolution equation, like Eq. (7). In principle the time to fracture  $t_c$  is a decreasing function of the applied tensile stress  $\sigma(t)$ . For a constant tensile stress  $\sigma_F$ , applied during the time interval  $t_c$  required for a spall, the critical number of microvoids is

$$(9) \quad N_c = \int_0^{t_c} g[\sigma(t)] dt \quad \text{and} \quad N_c = g(\sigma_F)t_c.$$

If  $N_c$  is a material constant then the spall criterion can be written as follows, [14]:

$$(10) \quad C = \int_0^{t_c} (\sigma - \sigma_{F0})^\delta dt \quad \text{and} \quad C = (\sigma_F - \sigma_{F0})^\delta t_c,$$

where the threshold stress  $\sigma_{F0}$ ,  $C$  and  $\delta$  are material constants. Some improvements of this criterion have been proposed by different authors, for example [19]. All criteria of spalling based on the overstress concept (with  $\sigma_{F0}$  being the measure of fracture stress at infinite time) can be implemented without difficulties into numerical codes. However, the overstress concept leads to an inconsistency at small differences between  $\sigma$  and  $\sigma_0$  because the critical times are excessively long. In addition, the constants are purely phenomenological.

A more plausible and simpler criteria, with the constants having some physical meaning, are based on Boltzmann statistics, [1, 20]. Every kinetic process, including spallation, must depend on temperature and rate of loading. The most straightforward approach to fracture and spallation is to use the theory of thermally activated processes, for example similar to that in dynamic plasticity, [21]. The common feature of this theory is that the rate  $\dot{a}$  of a system overcoming an energy barrier is given by

$$(11) \quad \dot{a} = \dot{a}_0 \exp\left(-\frac{\Delta G}{kT}\right),$$

where  $\dot{a}_0$  is the characteristic frequency (attempt frequency) of the system oscillating from an equilibrium position in front of the barrier, and  $\Delta G$  is the free energy difference between the equilibrium position and the maximum position (the saddle point) of the barrier. The term  $\exp(-\Delta G/kT)$  is linked to the probability that the system can be excited to a state of the free energy higher by  $\Delta G$ . In practice, the exact form of Eq. (11) is difficult to obtain for any thermally activated process. In case of spalling, Eq. (11) can be applied assuming that both the rate  $\dot{a}$  and the free energy  $\Delta G$  are functions of the normal stress  $\sigma$ , then

$$(12) \quad \dot{a}_0 = \dot{a}(\sigma) \exp\left(\frac{\Delta G(\sigma)}{kT}\right).$$

Both the frequency of separation and the free energy can be affected by the stress. Equation (12) can be an ample source of fracture criteria, [19, 21]. The most logical approach is to assume that the creation frequency, or the rate of microvoid evolution, has the form

$$(13) \quad \dot{N}_0 = \dot{N}(\sigma) \exp\left(\frac{\Delta G_0}{kT}\right),$$

where  $\Delta G_0$  is a constant energy of activation for this process,  $N(\sigma)$  is an increasing function of  $\sigma$ . A reasonable assumption in deriving a spall criterion is the constancy of the frequency factor  $\dot{a}$  combined with a very simple dependence of the free energy on stress (the so-called Yokobori's expression for the free energy):

$$(14) \quad \Delta G(\sigma) = \Delta G_0 \ln\left(\frac{\sigma}{\sigma_0}\right).$$

If Eq.(12) is combined with Eq.(14), the final form of the spall criterion is obtained, [1]

$$(15) \quad t_{c0} = \int_0^{t_c} \left(\frac{\sigma_F(t)}{\sigma_{F0}}\right)^{\alpha(T)} dt \quad \text{where} \quad \alpha(T) = \frac{\Delta G_0}{kT},$$

where at constant temperature  $T$ ,  $\sigma_{F0}$ ,  $t_{c0}$  and  $\alpha$  are three material constants,  $t_{c0}$  is the longest critical time when  $\sigma_F(t_{c0}) = \sigma_{F0}$ , for  $t_c > t_{c0}$ ,  $\sigma_F = \sigma_{F0}$ . The exponent  $\alpha(T)$  is temperature dependent and is related to the activation energy of material separation  $\Delta G_0$ . When the process is nonisothermal the exponent  $\alpha(T)$  is temperature and time-dependent,  $\alpha(T, t) = \Delta G_0/kT(t)$ , and Eq.(15) must be integrated accordingly. This cumulative criterion in the form of Eq.(15) has been proposed by KLEPACZKO, [1], and several forms of the  $\sigma(t)$  histories were analyzed in this reference. For the case of square pulse  $\sigma_F(t) = \sigma_F H(t)$ , where  $H(t)$  is the Heaviside step function and with the constant temperature, the criterion takes the form

$$(16) \quad \sigma_F(t_c) = \sigma_{F0} \left(\frac{t_{c0}}{t_c}\right)^{1/\alpha} \quad \text{and} \quad t_c = t_{c0} \left(\frac{\sigma_{F0}}{\sigma_F}\right)^\alpha.$$

The cumulative criterion, [15], is to some extent similar to the criterion for delayed yielding, CAMPBELL [22]. The cumulative criterion has been so far verified for some aluminum alloys. Here, the criterion will be directly applied to Al-alloy 7020-T6.

A series of plate impact tests have been performed on aluminum alloy 7020-T6 in order to determine the three constants in Eq.(15). The plate/plate configuration was used to produce a short tensile pulse of one-dimensional-strain in

a flat, round specimen. A flyer plate mounted on a cylindrical sabot is accelerated in a barrel by sudden release of pressurized gas, and impacts a target plate at a desired velocity. All plate impact experiments can be performed in vacuum at different impact velocities from  $50 \text{ ms}^{-1}$  to  $400 \text{ ms}^{-1}$ . The high pressure gas launcher is controlled entirely by a computer and an automaton. The impact velocity is the only parameter necessary to find the three constants after the analysis of the specimen cross-section. The results are shown in Fig. 7.

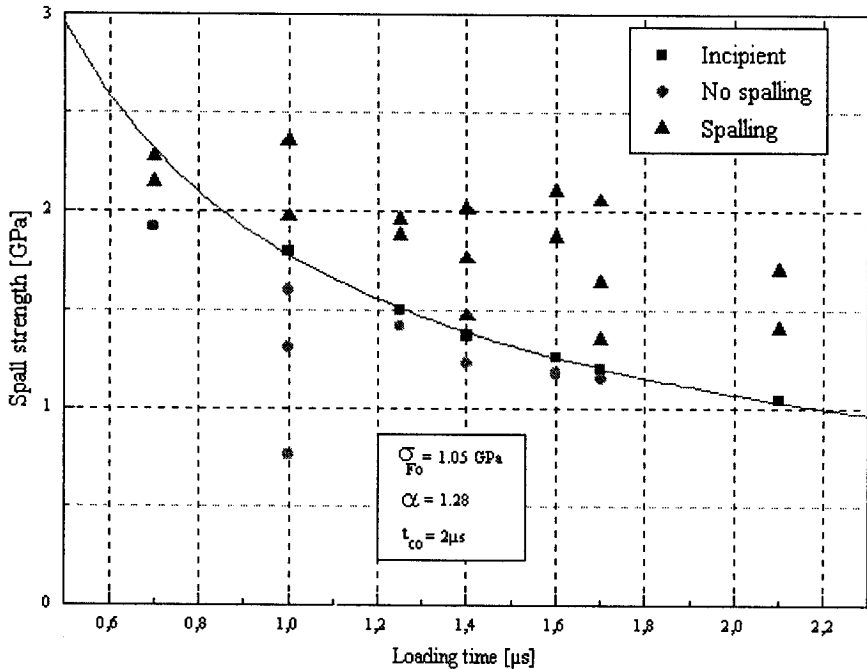


FIG. 7. Spall strength vs. critical loading time for aluminum alloy 7020-T6, the solid line in the spall criterion, Eq. (15).

Three stages of the spall zone could be identified after microscopic observation: no spalling, incipient, and a complete spall (free surface). To determine the level of damage, all target plates were cut and observed with an optical microscope (the cross-section). The free surface resulting from spalling were observed using Scanning Electron Microscopy (SEM) and the result is shown in Fig. 8. For aluminum alloys, one observes a ductile separation which is characterized by dimples. The microscopic observations of the perpendicular cross-sections have revealed the shear ligaments between the microvoids. The cross-section of 7020-T6 specimen with the shear ligament is shown in Fig. 9, [4].

Free surface resulting from spalling of Armco iron and low alloy steel observed by SEM are shown in Fig. 10 and Fig. 11.

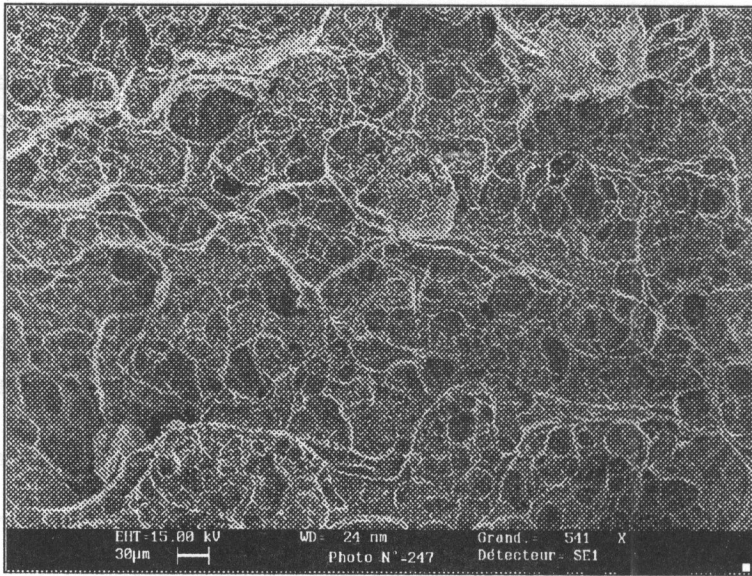


FIG. 8. Free surface of aluminum alloy 7020-T6 observed by SEM after spall, impact velocity  $V_0 = 280$  m/s.

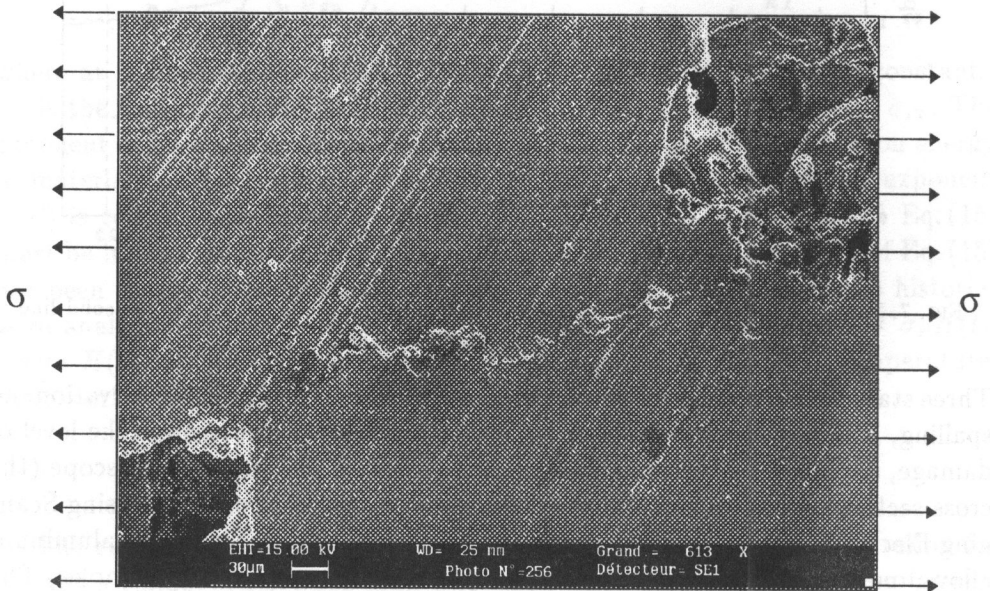


FIG. 9. Shear fracture (shear band) between two voids in aluminum alloy 7020-T6, metallographic examination.

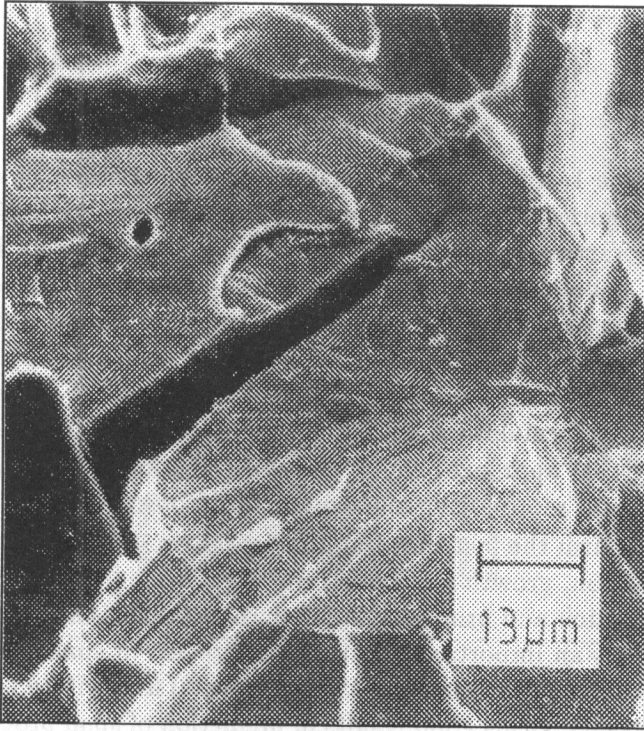


FIG. 10. Free surface of Armco iron observed by SEM after [4].

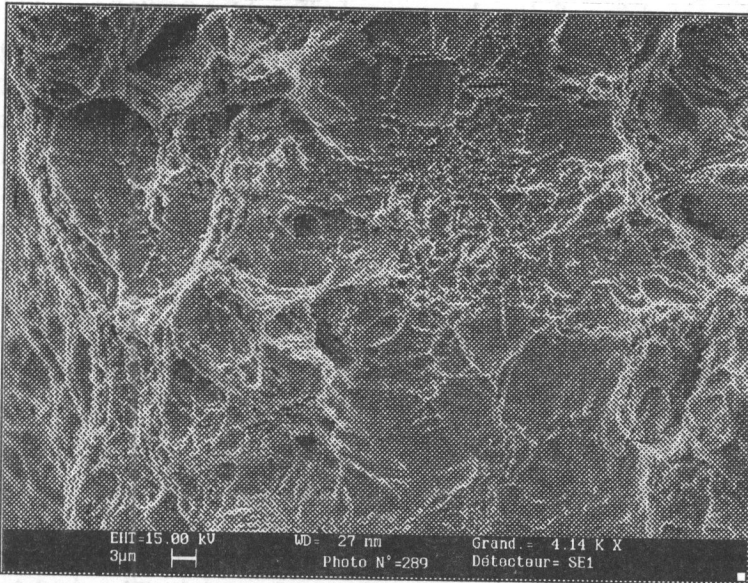


FIG. 11. Free surface of low alloy steel observed by SEM, steel tested after rolling,  $\approx 37$  HRC,  $V_0 = 350$  m/s.

## 6. DISCUSSION AND CONCLUSIONS

Following Table 1, it is possible to classify different criteria of spall and fracture in three categories. The first, corresponding to a micromechanical approach, which includes fracture mechanics, could be also applied to an isolated crack when the crack have large dimensions compared with the characteristic dimension of the microstructure. The second is a microstatistical approach, which results from statistical analysis of microdamage in specimens by counting and measuring the number of the microfractures (microcracks or microvoids). With such data one can formulate a statistical law of microfracture evolution. The third one is a global approach, where the considerations are phenomenological or based on physics, reproducing the experimental observations.

All studies confirm the fact that fracture process in ductile materials is due to microvoid nucleation, growth and coalescence, whereas in brittle materials, fracture is due to creation and propagation of microcracks. It is also well-known that microstructure has an important effect on the process of spallation. The simple criterion with a time delay (accumulation of defects) and with a limited number of material constants, yields good results in prediction of spall process. Moreover, criteria based on Boltzman statistics take into account the process of thermal activation and the delayed reaction of material, [1, 20, 23, 24]. Such criteria are easily implemented in a finite element code like ABAQUS\*R\* and they assure good results for variety of materials. Another criterion based on microstatistical approach has been developed around 1980, [10]. A physically-based model was proposed involving statistics of the nucleation, growth and coalescence of voids in a region undergoing tensile stresses (NAG model). This formulation is precise but the problem of specifying the complete material properties including the spectrum of microscopic voids and impurities is clearly formidable. In addition, this treatment is empirical and cannot be extrapolated with confidence to other materials and loading conditions. Recent progress in fractograph measurements will enable further advances in understanding of dynamic fracture, and in particular the mechanisms of nucleation, growth and coalescence which may lead to improvements of the NAG model, [16].

The most widely used constitutive relations for porous elastic-plastic solids are based on the work of GURSON, [6]. Gurson's considerations lead to a macroscopic yield condition and a flow rule in terms of the flow potential. Volume fraction of voids plays the role of an internal variable, which defines an evolution equation involving contributions by void nucleation and growth. The model of Gurson may have modifications, [25, 7, 26, 23, 27], where different porosity evolution is considered in the ductile process of fracture. Weaknesses of the porosity evolution models were revealed when the models were applied to predict the onset of

Table 1.

ref.	authors and year	mathematical formulation	constants	comments
[24]	Zhurkov (1965)	$\tau = \tau_0 \exp\left(\frac{u_0 - \gamma\sigma}{kT}\right)$	$\tau$ - time to fracture $\tau_0$ - characteristic time $u_0$ - binding energy $\gamma$ - activation volume	Boltzmann statistics, no cumulation
[14]	Tuler, Butcher (1968)	$t_{c0} = \int_0^{t_c} (\sigma_F - \sigma_{F0})^\delta dt$	$t_c$ - fracture time $\sigma_{F0}$ - stress below which fracture would not occur $\delta$ - constant	Overstress concept with time cumulation
[41]	Carroll, Holt (1972)	$\dot{\xi}_{\text{nucleation}} = \frac{h(\xi)}{1 - \xi} \left[ \exp\left(\frac{m_2 \sigma - \sigma_{N'} }{kT}\right) - 1 \right]$	$h(\xi)$ - material function of nucleation (effects of interactions of microvoids) $\xi$ - porosity parameter $\sigma_{N'}$ - threshold stress for the nucleation $m$ - material coefficient	Overstress concept with Boltzmann statistics
[42]	Johnson (1981)			
[23]	Perzyna (1986)			
[33]	Cagnoux (1985)	$\sigma_{\text{eff}} = \frac{\sigma}{1 - D}$ $\dot{D} = g(\sigma_{\text{eff}}, D)$ $D = \frac{1}{B} \int_{t_0}^t \left(\frac{\sigma - \sigma_0}{1 - D}\right)^\gamma (1 - D)^{\gamma - b(\sigma)}$	$D$ - damage parameter $\sigma_{\text{eff}}$ - effective stress $g$ - constant $b$ - function of $\sigma$	Damage evolution Cumulation of damage
[40]	Johnson, Cook (1985)	$D = \sum \frac{\Delta\epsilon}{\epsilon_f}$ $\epsilon_f = \left( D_1 + D_2 \exp\left(D_3 \frac{\sigma_m}{\sigma_{\text{eq}}}\right) \right) \times \left( 1 + D_4 \ln\left(\frac{\dot{\epsilon}}{\dot{\epsilon}_0}\right) \right) (1 + D_5 T^{**})$	$D$ - damage parameter $\epsilon_f$ - critical strain $D_1, D_2, D_3, D_4, D_5$ - constants which are determined from shear and tensile tests $\sigma_m = \text{tr}[\sigma]$ , average stress $\sigma_{\text{eq}}$ - equivalent stress $\dot{\epsilon}_0$ - reference strain rate	Damage evolution Critical strain criterion

Table 1 [cont.]

[19]	Letian, Yilong Shida (1986)	$F = 1 - \frac{\sigma_r}{\sigma_b}$	$\sigma_r$ - residual strength of spalled specimen $\sigma_b$ - ultimate tensile strength $F$ - damage function	Critical overstress
[20]	Dremin, Molodets (1986)	$\dot{\phi} = \tau_0^{-1} \exp\left(\frac{-u_0 + v_a \sigma_L}{kT}\right)$ $\int_0^\tau \dot{\phi} dt = 1$	$\tau$ - time necessary to accumulate the nuclei of flaw concentration up to the critical state $\tau_0$ - time constant $u_0$ - energy constant $\gamma$ - microstructural parameters $v_a$ - activation volume $\sigma_L$ - local stress $\dot{\phi}$ - accumulation rate of damage	Boltzmann statistics with time cumulation (improved Zhurkov criterion)
[31]	Speight, Taylor (1986)	$\sigma_{\max} > 2\sigma_F$ $\sigma_F = \frac{1}{2} \rho c_1 \Delta v$	$\Delta v$ - pullback velocity, which is measured with a VISAR, for example $\sigma_F$ - critical stress	Critical stress criterion with residual velocity
[29]	Zhou, Cheng (1988)		$D(x, t)$ - damage function $dv$ - volumetric variation of material $A$ - unit area $t^*$ - time of reaching maximum tensile stress	Damage evolution $D(x, t)$ - damage function
[32]	Cochran, Banner (1977)	$D(x, t) = \int_{t^*}^t \frac{dv}{A}$ $F(x, t) = 1 - \left(\frac{D(x, t)}{D_0}\right)^{2/3}$ $\sigma = F\Sigma$	$F$ - strength function $D_0$ - critical value of damage corresponding to complete spalling $\sigma$ - true stress $\Sigma$ - strength of spallation	
[9]	Shockey		$N$ - number of cavities with a radius greater than $R$	Microstatistics, time evolution, cumulation of voids
[10]	Seaman	$N = N_0 \exp\left(-\frac{R}{R_1}\right)$	$N_0$ - total number of cavities studied	
[18]	Curran (1980-1995)	$\dot{R} = \frac{\sigma - \sigma_{y0}}{4\eta} R$	$\eta$ - viscosity parameter $R_1$ - distribution characteristic	

Table 1 [cont.]

[25]	Klöcker Montheillet (1988)	$\frac{R}{R_0} = \exp\left(\frac{\dot{\epsilon} - \dot{\epsilon}}{2}\right) \frac{t}{\dot{\epsilon} \sqrt{3\dot{\epsilon}}}$ $\zeta = \frac{1}{3} + 1/\sqrt{3} \int_0^t (1+x^2)^{m-1/2} dx$	$t_{co} = \int_0^{t_c} \left(\frac{\sigma_F(t)}{\sigma_{F0}}\right)^{\alpha(T)} dt$ $\alpha(T) = \frac{\Delta H}{kT}$	$\zeta = \frac{1}{3} + 1/\sqrt{3} \int_0^t (1+x^2)^{m-1/2} dx$	$R$ - void radius $R_0$ - initial radius $\dot{\epsilon}$ - depends on the triaxiality $\zeta$ $\dot{\epsilon}$ - tensile strain rate $\zeta$ - triaxiality ratio $m$ - rate sensitivity	Statistics, cumulation of voids
[1]	Klepaczko (1990)	$t_{co} = \int_0^{t_c} \left(\frac{\sigma_F(t)}{\sigma_{F0}}\right)^{\alpha(T)} dt$ $\alpha(T) = \frac{\Delta H}{kT}$	$t_{co} = \int_0^{t_c} \left(\frac{\sigma_F(t)}{\sigma_{F0}}\right)^{\alpha(T)} dt$	$t_{co}$ - longest critical time $\sigma_{F0}$ - material constant $\alpha$ - function of temperature $T$ - temperature $\Delta H$ - free enthalpy $k$ - Boltzmann constant	Boltzmann statistics with time cumulation	
[35] [6], [28] [34]	Grady (1987) Gurson (1975 - 1977) Buchar, Krejci (1994)	brittle materials $\sigma_c = (3\rho c_0 K_c^2 \dot{\epsilon})^{1/3}$ ductile materials $\sigma_c = (2Y \rho c_0^2 \dot{\epsilon}_v)^{1/2}$		$\sigma_c$ - spall strength $K_c$ - fracture toughness $Y$ - flow stress $\dot{\epsilon}_v$ - critical void fraction	Critical stress concept, no cumulation	
[13]	Kanel (Fortov, Kostin, Eliezer) (1991)	$\frac{dV_t}{dt} = -k \sin(P) (\sigma_{\max} - \sigma_{0e}) (V_t + V_{t1})$ $\frac{dV_t}{dt} = 0 \quad \text{if }  \sigma_{\max}  < \sigma_{0e}$		$V_t$ - specific volume of microvoids $k$ - constant $V_{t1}$ - critical value of $V_t$ $\sigma_{0e}$ - threshold stress $\sigma_{\max}$ - maximum stress	Statistics Cumulation of defect	
[36]	Petrov, Morozov (1994)	$\frac{1}{\tau} \int_{t-\tau}^t \frac{1}{d} \int_0^d \sigma(r, t') dr dt' \leq \sigma_c$		$\sigma_c$ - static strength of the material $d$ - critical size of flaw $t$ - critical time $\sigma(r, t)$ - maximum tensile stress in the process zone	Critical stress with time cumulation	

strain localization as a consequence of a constitutive formulation. Therefore some improvements were suggested to introduce two adjustable parameters  $q_1$  and  $q_2$  into the GURSON model, [28]. This modification still did not describe the rapid loss of strength near the final failure when the ligaments between the voids start to collapse. Further refinements were proposed, [15], to enhance the effect of porosity in the constitutive formulation by using a variable instead of the void volume fraction, and by letting this variable grow faster than void volume fraction near the final stage of fracture. In general, the void growth models were used in limited cases to calculate numerically spall damage, [29, 30, 25, 7, 26, 15].

The results of the numerical simulations of spall experiments in aluminum alloys, copper and steels show that by using relatively simple criteria, it is possible to predict relatively well the main features of spall fracture in ductile as well as in brittle metals. However, it should be kept in mind that the validity of the calculations is mainly limited by the accuracy of the constants included in the spall criteria. Furthermore, it is important to develop spall criteria which take explicitly into account the effect of microstructure in the spall condition, since the microstructure is the key factor in the dynamic fracture processes.

#### REFERENCES

1. J.R. KLEPACZKO, *Dynamic crack initiation. Some experimental methods and modelling*, [in:] Crack Dynamics in Metallic Materials, J.R. KLEPACZKO [Ed.], Springer-Verlag, Vienna-New-York 428, 1990.
2. A.A. GRIFFITH, *The phenomenon of rupture and flow in solids*, Phil. Trans. Roy. Soc., London, **A 221**, 163, 1921.
3. J.J. GILMAN, *Monocrystals in mechanical technology*, Trans. Quart. ASM, **59**, 596, 1966.
4. W. ARNOLD, *Dynamisches Werkstoffverhalten von Armco-Eisen bei Stosswellenbelastung*, Fortschritt-Berichte VDI, Reihe, **5**, 247, 1992.
5. P. CHEVRIER, *Etude de l'endommagement dynamique d'alliages d'aluminium soumis à une onde plane induite par un impact plaque sur plaque-Technique expérimentale*, DEA Report, 1994.
6. A.L. GURSON, *Continuum theory of ductile rupture by void nucleation and growth, Part I. Yield criteria and flow rules for porous ductile media*, J. Engng. Mater. Tech., **99**, 2, 1977.
7. J. EFTIS and J.A. NEMES, *Constitutive modelling of spall fracture*, Arch. Mech., **43**, 399, 1991.
8. A. PINEAU, *Effect of inhomogeneities in the modelling of mechanical behaviour and damage of metallic materials*, [in:] Mechanical Behaviour of Materials, ESIS, Delft University Press, Delft 1995.
9. D.R. CURRAN, *Microstatistical fracture mechanics in dynamic fracture*, [in:] Crack Dynamics in Metallic Materials, p. 455, J.R. KLEPACZKO [Ed.], Springer Verlag, 1990.

10. D.A. SHOCKEY, L. SEAMAN and D.R. CURRAN, *Linking dynamic fracture to microstructural processes*, [in:] Shock Waves and High Strain Rate Phenomena in Metals, p. 129, M.M. MEYERS and L.E. MURR [Eds.], Plenum Press, N. Y. 1981.
11. R.F. ROLSTEN, *A study of the shock loading of materials*, Trans. N.Y. Acad. Sci., **36**, 416, 1974.
12. M. LACOMME, B. CAZALIS, J. DAVID, G. NIERAT, A. SALÈRES and G. SIBILLE, *Endommagement et écaillage par laser*, J. Physique, **4**, 77, 1994.
13. V.E. FORTOV, V.V. KOSTIN and S. ELIEZER, *Spallation of metals under laser irradiation*, J. Appl. Phys., **70**, 4524, 1991.
14. F.R. TULER and B.M. BUTCHER, *A criterion for the time dependence of dynamic fracture*, Int. J. Fract. Mech., **4**, 431, 1968.
15. M.J. WORSWICK, H. NAHME and J. FOWLER, *Spall through void nucleation, growth and coalescence*, J. Physique, **4**, C8-623, 1994.
16. B. YILONG, K. FUJII and L. LIMIN, *Statistical modelling of damage evolution in spallation*, J. Physique, **49**, C3, 215, 1988.
17. C. DUMONT and C. LEVAILLANT, *Croissance de cavités dans des matériaux à matrice ductile*, DYMAT 6<sup>ième</sup> Journée Nationale, **2**, 1, 1990.
18. D.A. SHOCKEY, *Understanding dynamic fracture phenomenology with fractography*, [in:] Metallurgical and Materials Applications of Shock-Wave and High-Strain-Rate Phenomena, 151, 1995.
19. S. LETIAN, B. YILONG and Z. SHIDA, *Experimental study of spall damage in an aluminum alloy*, Proc. Intern. Symposium on Intense Dynamic Loading and its Effects, China, 753, 1986.
20. A.N. DREMIN and A.M. MOLODETS, *On the spall strength of metals*, Proc. Intern. Symposium on Intense Dynamic Loading and its Effects, Science Press, Beijing, China, 13, 1986.
21. L. DAVIDSON and M.E. KIPP, *Calculation of spall damage accumulation in ductile metals*, [in:] High Velocity Deformation of Solids, p. 163, K. KAWATA and J. SHIORI [Eds.], Springer, New York 1978.
22. J.D. CAMPBELL, *Dynamic plasticity*, Springer Verlag, 1966.
23. P. PERZYNA, *Internal state variable description of dynamic fracture of ductile solids*, Int. J. Solids Structures, **22**, 797, 1986.
24. S.N. ZHURKOV, *Kinetic concept of the strength of solids*, Int. J. Fract. Mech., **1**, 311, 1965.
25. H. KLÖCKER and F. MONTHEILLET, *Modeling the ductile growth of voids at high strain rates*, J. Physique, **49**, C3-9, 313, 1988.
26. I.M. FYFE, *Application of Gurson void growth model to dynamic fracture*, [in:] Materials Behaviour Under High Stress and Ultra High Loading Rates, p. 309, J. MESCALL and V. WEISS [Eds.], Plenum, New York 1982.
27. V. TVERGAARD, *Micromechanics of damage in metals*, [in:] Mechanical Behaviour of Materials,ESIS, Delft University Press, Delft 1955.
28. A.L. GURSON, *Plastic flow and fracture of ductile materials incorporating void nucleation, growth and interaction*, Ph. D. Thesis, Brown University, 1975.

29. G.O. ZHOU and J.Y. CHENG, *Dynamic-active constitutive relations with damage* [Private communication].
30. H. NAHME and M.J. WORSWICK, *Dynamic properties and spall plane formation of brass*, J. Physique, **4**, C8-707, 1994.
31. C.S. SPEIGHT and P.F. TAYLOR, *Dynamic fracture criteria from free surface velocity measurements*, [in:] Metallurgical Applications of Shock-Wave and High-Strain-Rate Phenomena, p. 805, MURR, STAUDHAMMER, MEYERS [Eds.], Marcel Dekker Inc., 1986.
32. S. COCHRAN and D. BANNER, *Spall studies in uranium*, J. Appl. Phys., **48**, 2729, 1977.
33. J. CAGNOUX, *Déformation et ruine d'un verre pyrex soumis à un choc intense: Etude expérimentale et modélisation du comportement*, Ph. D. Thesis, Poitiers University, 1985.
34. J. BUCHAR and J. KREJCI, *Spall behaviour of the low alloyed high strength steel*, J. Physique, **4**, C8, 713, 1994.
35. D.E. GRADY, *The spall strength of condensed matter*, J. Mech. Phys. Solids, **36**, 353, 1988.
36. Y.V. PETROV and N.F. MOROZOV, *On the modeling of fracture of brittle solids*, J. Appl. Mech., **61**, 710, 1994.
37. L.M. BARKER and R.E. HOLLENBACH, *Laser interferometer for measuring high velocities of any reflecting surface*, J. Appl. Phys., **43**, 4669, 1972.
38. L. DAVISON and A.L. STEVENS, *Continuum measures of spall damage*, J. Appl. Phys., **43**, 988, 1972.
39. J.S. RINEHART, *Scabbing of metals under explosive attack: multiple scabbing*, J. Appl. Phys., **23**, 1229, 1952.
40. J.N. JOHNSON and W.H. COOK, Engng. Fract. Mech., **21**, 31, 1985.
41. M.M. CARROLL and A.C. HOLT, *Static and dynamic pore-collapse relations for ductile porous materials*, J. Appl. Phys., **43**, 1626, 1972.
42. J.N. JOHNSON, *Dynamic fracture and spallation in ductile solids*, J. Appl. Phys., **52**, 2812, 1981.

LABORATOIRE DE PHYSIQUE ET MECANIQUE DES MATERIAUX  
INSTITUT SUPERIEUR DE GENIE MECANIQUE ET PRODUCTIQUE  
UNIVERSITE DE METZ, METZ, FRANCE

e-mail: chevrier@lpmm.univ-metz.fr

Received September 2, 1996.

---